

The role of GpsB in *Staphylococcus aureus* cell morphogenesis

Sara F. Costa,¹ Bruno M. Saraiva,¹ Helena Veiga,¹ Leonor B. Marques,¹ Simon Schäper,¹ Marta Sporniak,¹ Daniel E. Vega,¹ Ana M. Jorge,¹ Andreia M. Duarte,¹ António D. Brito,¹ Andreia C. Tavares,¹ Patricia Reed,¹ Mariana G. Pinho¹

AUTHOR AFFILIATION See affiliation list on p. 13.

ABSTRACT For decades, cells of the Gram-positive bacterial pathogen *Staphylococcus aureus* were thought to lack a dedicated elongation machinery. However, *S. aureus* cells were recently shown to elongate before division, in a process that requires a shape elongation division and sporulation (SEDS)/penicillin-binding protein (PBP) pair for peptidoglycan synthesis, consisting of the glycosyltransferase RodA and the transpeptidase PBP3. In ovococci and rod-shaped bacteria, the elongation machinery, or elongasome, is composed of various proteins besides a dedicated SEDS/PBP pair. To identify proteins required for *S. aureus* elongation, we screened the Nebraska Transposon Mutant Library, which contains transposon mutants in virtually all non-essential staphylococcal genes, for mutants with modified cell shape. We confirmed the roles of RodA/PBP3 in *S. aureus* elongation and identified GpsB, SsaA, and RodZ as additional proteins involved in this process. The *gpsB* mutant showed the strongest phenotype, mediated by the partial delocalization from the division septum of PBP2 and PBP4, two penicillin-binding proteins that synthesize and cross-link peptidoglycan. Increased levels of these PBPs at the cell periphery versus the septum result in higher levels of peptidoglycan insertion/crosslinking throughout the entire cell, possibly overriding the RodA/PBP3-mediated peptidoglycan synthesis at the outer edge of the septum and/or increasing stiffness of the peripheral wall, impairing elongation. Consequently, in the absence of GpsB, *S. aureus* cells become more spherical. We propose that GpsB has a role in the spatio-temporal regulation of PBP2 and PBP4 at the septum versus cell periphery, contributing to the maintenance of the correct cell morphology in *S. aureus*.

IMPORTANCE *Staphylococcus aureus* is a Gram-positive clinical pathogen, which is currently the second cause of death by antibiotic-resistant infections worldwide. For decades, *S. aureus* cells were thought to be spherical and lack the ability to undergo elongation. However, super-resolution microscopy techniques allowed us to observe the minor morphological changes that occur during the cell cycle of this pathogen, including cell elongation. *S. aureus* elongation is not required for normal growth in laboratory conditions. However, it seems to be essential in the context of some infections, such as osteomyelitis, during which *S. aureus* cells apparently elongate to invade small channels in the bones. In this work, we uncovered new determinants required for *S. aureus* cell elongation. In particular, we show that GpsB has an important role in the spatio-temporal regulation of PBP2 and PBP4, two proteins involved in peptidoglycan synthesis, contributing to the maintenance of the correct cell morphology in *S. aureus*.

KEYWORDS *Staphylococcus aureus*, elongasome, GpsB, morphogenesis

Staphylococcus aureus is a Gram-positive bacterial pathogen, responsible for a high number of antibiotic-resistant infections, and is currently the second major cause of death by antibiotic-resistant infections (1). For decades, *S. aureus* cells were thought to lack a dedicated elongation machinery, and *S. aureus* was often mentioned as a canonical example of truly spherical cocci. Rods, which have a cylindrical shape, undergo

Editor N. Luisa Hiller, Carnegie Mellon University, Pittsburgh, Pennsylvania, USA

Address correspondence to Mariana G. Pinho, mgpinho@itqb.unl.pt.

Sara F. Costa, Bruno M. Saraiva, Helena Veiga, and Leonor B. Marques contributed equally to this article. The author order was determined by their contribution to the article.

The authors declare no conflict of interest.

See the funding table on p. 13.

Received 13 December 2023

Accepted 20 December 2023

Published 6 February 2024

Copyright © 2024 Costa et al. This is an open-access article distributed under the terms of the [Creative Commons Attribution 4.0 International license](https://creativecommons.org/licenses/by/4.0/).

cell elongation before the synthesis of a septum that divides the mother cell in two identical daughter cells. In these organisms, cell elongation and division are organized by two cytoskeletal proteins, the bacterial actin homolog MreB and the tubulin homolog FtsZ, respectively, which coordinate the assembly of two multiprotein complexes, the elongasome or Rod complex and the divisome (2–4). These complexes include cell wall synthesis proteins and organize synthesis of new peptidoglycan at the lateral wall and at the division septum.

S. aureus cells lack an MreB homolog and were previously thought to lack a canonical elongasome (5). The view that *S. aureus* had only one cell wall synthesis machinery that made peptidoglycan at the division septum was present in work by G. Satta in the 1990s (6). This work proposed a “two-competing-sites model” for peptidoglycan assembly which predicted that there were two types of cocci: one that synthesized peptidoglycan only at the septum (which would include *S. aureus*) and another that also synthesized peptidoglycan for lateral wall elongation (which would include ovococci such as *Enterococcus faecium* or *Streptococcus agalactiae*) (6). In these studies, *S. aureus* was unable to elongate under various conditions that promoted elongation of ovococci, such as the presence of antibiotics that inhibit septation (6). However, the recent development of super-resolution microscopy techniques allowed imaging of the small (~1 μm in diameter) staphylococcal cells, with sufficient resolution to observe minor morphological changes that occur during the cell cycle. This showed that *S. aureus* cells do undergo slight elongation, which is reflected in an increase in the ratio of the longer cell axis (perpendicular to the division septum) to the shorter cell axis (overlapping the septum) during the cell cycle (7). The *S. aureus* cell cycle can be divided in three different phases: phase 1, before initiation of division septum synthesis; phase 2, during which septum synthesis occurs; and phase 3, during which cells have a complete septum, undergoing maturation, before splitting in two identical daughter cells (7). Cell volume increases during the entire cell cycle, while cell elongation occurs mostly during phases 1 and 3 (7). We have recently shown that this elongation process is dependent on the presence of the shape elongation division and sporulation (SEDS)/penicillin-binding protein (PBP) pair RodA/PBP3, proteins with glycosyltransferase activity responsible for glycan strand synthesis and transpeptidase activity responsible for peptidoglycan crosslinking, respectively (8). Together, these proteins catalyze peptidoglycan synthesis, including at the sidewall of the septal region, resulting in slight cell elongation (8). This midcell synthesis is reminiscent to that observed in ovococoid bacteria such as *Streptococcus pneumoniae*, which also lack an MreB homolog (9, 10), but different from elongation of rod-shaped bacteria such as *Escherichia coli* or *Bacillus subtilis* where MreB polymerizes into short filaments that move processively in a circumferential direction, perpendicular to the long axis of the rod, organizing the elongasome machinery and leading to peptidoglycan incorporation over the entire length of the cell (11–13). Besides having a dedicated SEDS/PBP pair, rod elongasome also includes two transmembrane proteins, MreC and MreD, proposed to couple intracellular MreB to extracellular PBPs (14) and RodZ, which interacts with other elongasome components (15) and may modulate MreB filament density (16).

Given the relative complexity of elongasomes in rods, it seemed unlikely that elongation in *S. aureus* would require just RodA and PBP3, the only two proteins so far identified as having a role in this process. We hypothesized that *S. aureus* elongation was not essential during growth in rich medium, as deletion of both *rodA* and *pbp3* (previously called *pbpC*) genes was not lethal in these conditions (8). Therefore, to identify additional factors required for *S. aureus* elongation, we screened by microscopy the Nebraska Transposon Mutant Library (NTML), composed of mutants with a *bursa aurealis* transposon insertion in virtually every non-essential gene of the methicillin-resistant *S. aureus* (MRSA) strain JE2 (17), for mutants with cells with decreased eccentricity.

MATERIALS AND METHODS

Bacterial growth conditions

S. aureus strains were grown at 37°C in tryptic soy broth (TSB, Difco) with agitation or on plates of tryptic soy agar (Difco). When necessary, culture media were supplemented with appropriate antibiotics chloramphenicol 10 µg/mL, erythromycin 10 µg/mL (Sigma-Aldrich, during intermediate step in the construction of deletion mutants) or erythromycin 25 µg/mL (NTML mutants), kanamycin 150 µg/mL (Apollo Scientific, overnight cultures) or 50 µg/mL (cultures for microscopy), or a combination of kanamycin (50 µg/mL) with neomycin (50 µg/mL, Apollo Scientific), with 100 µg/mL 5-bromo-4-chloro-3-indolyl-β-D-galactopyranoside (X-Gal, VWR), or with 0.1 µM CdCl₂ (Sigma-Aldrich). *E. coli* strains were grown at 37°C in Luria-Bertani broth (LB, Difco) or on LB agar (Difco) supplemented with ampicillin 100 µg/mL (Sigma-Aldrich) when required.

Microscopy screening of the NTML

Batches of 48 mutants of the NTML (17) were imaged, with parental strain JE2 imaged before and after the first and last groups of eight mutants, respectively. Each strain was grown overnight at 37°C in TSB supplemented with erythromycin 25 µg/mL, except for JE2 which was grown without antibiotic. Each overnight culture was back diluted 1:200 in TSB and grown to an OD₆₀₀ of 0.8. From each culture, a 300 µL aliquot was incubated with 0.4 µL of both Nile red (10 mg/mL, Invitrogen) and Hoechst 33342 (5 mg/mL, Invitrogen) for 5 min at 37°C with shaking. Samples were pelleted and resuspended in 10 µL of a solution of 1:3 (vol/vol) TSB/phosphate-buffered saline (PBS, NaCl 137 mM, KCl 2.7 mM, Na₂HPO₄ 10 mM, KH₂PO₄ 1.8 mM). One microliter of each sample was mounted on a layer of 1.2% (wt/vol) agarose in 1:3 (vol/vol) TSB/PBS placed on a glass plate (Bio-Rad Mini-PROTEAN Short Plate) with a coverslip placed on top of each sample. Eight samples were imaged per glass plate, using a Zeiss Axio Observer microscope equipped with a Plan-Apochromat 100×/1.4 oil Ph3 objective, a Retiga R1 CCD camera (QImaging), a white-light source HXP 120 V (Zeiss), and Metamorph 7.5 software (Molecular Devices). The filters (Semrock) Brightline TXRED-4040B (Nile red) and Brightline DAPI-1160A (Hoechst 33342) were used for image acquisition. Phase contrast and widefield fluorescence microscopy images (minimum of five fields of view per mutant) were acquired with an exposure time of 100 ms for all channels.

Analysis of cell morphology of NTML mutants

The eHooke software (18) was used to automatically perform image segmentation of cells from each mutant (at least five fields of view per mutant) and to measure morphological parameters of individual cells, namely, area, perimeter, axis sizes, eccentricity, and irregularity. This was followed by a visual inspection of the images by at least two users to qualitatively evaluate the quality of segmentation results. Data from images that were not correctly segmented were not considered for further analysis. Mutants were ranked by eccentricity values (which can theoretically vary between 0 and 1), calculated according to equation 1, where “a” and “b” are the semi-major and semi-minor axes, respectively, defined as the major and minor axes of the smallest rectangle that can contain each cell (18).

$$\text{Eccentricity} = \sqrt{1 - \frac{b^2}{a^2}} \quad (\text{equation 1})$$

Construction of plasmids and bacterial strains

The plasmids and bacterial strains used in this study are described in Tables S1 and S2, respectively. The primers used are listed in Table S3.

Deletion mutants were constructed using the thermosensitive plasmid pMAD (19). The upstream and downstream regions of the genes SAUSA300_1090,

SAUSA300_2249 (*ssaA*), SAUSA300_0128, SAUSA300_1337 (*gpsB*), SAUSA300_1113 (*pknB*), SAUSA300_1175 (*rodZ*), and SAUSA300_0629 (*pbp4*) were amplified from *S. aureus* genomic DNA using the primers identified in Table S3. Subsequently, these fragments were cloned into pMAD plasmid in the *Sma*I site, in *E. coli* DC10B, using NEBuilder HiFi DNA assembly mix (New England BioLabs) through the Gibson assembly technique (20) creating pMAD- Δ 1090, pMAD- Δ ssaA, pMAD- Δ 0128, and pMAD- Δ pknB (see Table S1). For pMAD- Δ gpsB, pMAD- Δ rodZ, and pMAD-PBP4-KO, the amplified upstream and downstream regions were joined by overlap PCR and cloned into pMAD using the restriction sites *Nco*I/*Bam*HI or *Eco*RI/*Nco*I. Plasmids pMAD- Δ pbpC (8), pMAD- Δ rodA (8), p Δ mreD (21), and p Δ mreC (21) were already available.

The plasmids were extracted using a miniprep kit (NZYTech); the constructs were confirmed by Sanger sequencing (STAB VIDA) and then electroporated into *S. aureus* RN4220 at 30°C using erythromycin and X-gal selection (22). Blue colonies were selected to produce a phage lysate using phage 80 α (23), and the plasmids were transduced to *S. aureus* JE2 or COL. Constructs were integrated into the chromosome at 43°C, as previously described (19). Cells were then incubated at 30°C, and colonies where the plasmid had undergone excision were selected and tested by PCR, resulting in strains JE2 Δ 1090, JE2 Δ ssaA, JE2 Δ pbpC, JE2 Δ rodA, JE2 Δ 0128, JE2 Δ mreD, JE2 Δ gpsB, JE2 Δ pknB, JE2 Δ mreC, JE2 Δ rodZ, JE2 Δ pbp4, and COL Δ pbp4. Using the same procedure, pMAD- Δ gpsB vector was transduced into strains COL, COL Δ pbp4, ColsGFP-PBP1 (24), BCbPM073 (25), ColsGFP-PBP3 (24), COLpPBP4-YFP (26), and COL *EzrA*-sGFP (27) to delete *gpsB*, resulting, respectively, in strains COL Δ gpsB, COL Δ pbp4 Δ gpsB, ColsGFP-PBP1 Δ gpsB, ColsGFP-PBP2 Δ gpsB, ColsGFP-PBP3 Δ gpsB, COLpPBP4-YFP Δ gpsB, and COL *EzrA*-sGFP Δ gpsB. Deletion of each gene was confirmed by PCR using primers in Table S3 followed by Sanger sequencing, across the deleted region.

To complement the deletion mutants with plasmid-encoded copies of the corresponding genes, each gene was amplified by PCR, using primers indicated in Table S3, and cloned into the pCNX (7) or pCN51 (28) plasmid under the control of *P*_{cad} promoter, using restriction enzymes *Sma*I and *Eco*RI for *mreC* and *mreD* fragments and NEBuilder HiFi DNA assembly mix (New England BioLabs), in the *Sma*I restriction site, through the Gibson assembly technique (20) for the remaining fragments. The following plasmids were constructed: pCNX1090, pCNXssaA, pCNX0128, pCNXmreD, pCNXgpsB, pCN51gpsB, pCNXpknB, pCNXmreC, pCNXrodZ, and pBCbPM115 (pCNX encoding *pbp4*) (see Table S1). After confirmation of the insert sequence in pCNX or pCN51 by PCR and Sanger sequencing, DNA of plasmids with the correct insert was extracted and electroporated into *S. aureus* RN4220 at 37°C using kanamycin and erythromycin selection, respectively (22). Each plasmid was then transduced into the corresponding deletion mutant using phage 80 α , generating JE2 Δ 1090 pCNX1090, JE2 Δ ssaA pCNXssaA, JE2 Δ 0128 pCNX0128, JE2 Δ mreD pCNXmreD, JE2 Δ gpsB pCNXgpsB, JE2 Δ pknB pCNXpknB, JE2 Δ mreC pCNXmreC, JE2 Δ rodZ pCNXrodZ, JE2 Δ pbp4 pCNXpbp4, and COL Δ gpsB pCNXgpsB. As a control, the pCNX empty vector was transduced into *S. aureus* JE2 strain, generating JE2 pCNX. Strains ColsGFP-PBP2 Δ gpsB pCNXgpsB and ColsGFP-PBP2 pCNXgpsB were obtained by transducing plasmid pCNXgpsB into ColsGFP-PBP2 Δ gpsB and ColsGFP-PBP2, respectively. Strains COLpPBP4-YFP Δ gpsB pCN51gpsB and COLpPBP4-YFP pCN51gpsB were obtained by transducing plasmid pCN51gpsB into COLpPBP4-YFP Δ gpsB and COLpPBP4-YFP, respectively.

Analysis of *S. aureus* growth

The growth of COL, COL Δ gpsB, JE2, and JE2 Δ gpsB strains was analyzed in a 96-well plate reader (Biotek Synergy Neo2). Overnight cultures were diluted 1:1,000 in fresh media, 200 μ L of each culture were added to wells of a 96-well plate, and growth was followed at 37°C with agitation for 18 ½ hours. The OD₆₀₀ was measured every 30 min.

Fluorescence microscopy and cell morphology image analysis

For imaging, *S. aureus* strains were grown overnight at 37°C in TSB with selective antibiotics, diluted to an OD₆₀₀ of 0.05, and grown at 37°C with selective antibiotics and appropriate inducers until cultures reached an OD₆₀₀ of 0.5–0.6. When required, cells were labeled for 5 min at 37°C, with agitation, with DNA dye Hoechst 33342 (1 µg/mL, Invitrogen) and membrane dye Nile Red (5 µg/mL, Invitrogen). The cells were centrifuged for 1 min at 10,000 rpm in a benchtop centrifuge (Eppendorf 5430) and resuspended in PBS, and 1 µL of this cell suspension was placed onto a gel pad composed of 1.2% agarose (TopVision, Thermo Fisher Scientific) prepared in PBS and mounted on a microscopy slide.

Images were acquired with a Zeiss Axio Observer Z1 microscope equipped with a Plan-Apochromat 100×/1.40 oil Ph3 objective with numerical aperture 0.55, HXP 120 V Illuminator (Zeiss), and Photometrics CoolSNAP HQ camera (Roper Scientific, Inc.) and controlled by a ZEN software (Zeiss). The filters Brightline TXRED-4040B and Brightline DAPI-1160A (Semrock) were used for image acquisition of cells labeled with Nile red and Hoechst 33342, respectively. Phase-contrast images and widefield microscopy images were acquired with 100 ms exposure time. At least 10 images per mutant were acquired, and three biological replicates were performed for each mutant.

Automated analysis of microscopy images was performed using eHooke (18) to measure morphological parameters, including cell eccentricity, and to automatically assign the cell cycle phase to each analyzed cell. Eccentricity was calculated using Equation 1 described above. Data were plotted using GraphPad Prism 8 (GraphPad Software).

Assessment of FtsZ dynamics

To measure FtsZ treadmilling speed, COL EzrA-sGFP and COL EzrA-sGFP Δ *gpsB* strains were grown overnight, in triplicate, in TSB and diluted 1:200 in fresh TSB followed by incubation with shaking at 37°C. Exponentially growing cells (OD₆₀₀ of 0.6–0.8) were harvested by centrifugation for 1 min at 9,300 × *g*, resuspended in 30 µL fresh TSB, and spotted on a pad of 1.5% molecular biology grade agarose (Bio-Rad) in M9 minimal medium (KH₂PO₄ 3.4 g/L, VWR; K₂HPO₄ 2.9 g/L, VWR; di-ammonium citrate 0.7 g/L, Sigma-Aldrich; sodium acetate 0.26 g/L, Merck; glucose 1% [wt/vol], Merck; MgSO₄ 0.7 mg/L, Sigma-Aldrich; CaCl₂ 7 mg/L, Sigma-Aldrich; casamino acids 1% [wt/vol], Difco; MEM amino acids 1×, Thermo Fisher Scientific; MEM vitamins 1×, Thermo Fisher Scientific) mounted in a Gene Frame (Thermo Fisher Scientific) on a microscope slide. Imaging was performed in a DeltaVision OMX SR microscope equipped with a hardware-based focus stability (HW UltimateFocus) and an environmental control module set to 37°C. Z-stacks of three images with a step size of 500 nm were acquired every 3 seconds for 3 min using a 488-nm laser (100 mW, at 10% maximal power) with an exposure time of 50 ms. Maximum intensity projection (MIP) of three images from each Z-stack and subsequent image deconvolution were performed for each time frame in the software SoftWoRx. All 61 time frames were aligned using NanoJ-Core drift correction (29) and then used to perform MIP for the drawing of 1-pixel freehand lines over EzrA-sGFP signal in images of newborn sister cells that are still attached via the septum of the mother cell, in which nascent Z-rings appear sparse and Dshaped. Space-time kymographs were generated by extracting fluorescence intensities from individual time frames along drawn freehand lines using the software Fiji (30, 31). FtsZ treadmilling speed was calculated (in nanometers per second) by determining the slope of diagonals spanning the entire width of generated kymographs.

Analysis of the localization of PBPs and of peptidoglycan synthesis

To localize fluorescent derivatives of PBPs 1–4, strains ColsGFP-PBP1, BCBPM073 (encoding sGFP-PBP2), ColsGFP-PBP3, and COLpPBP4-YFP, the corresponding *gpsB* deletion mutants ColsGFP-PBP1 Δ *gpsB*, ColsGFP-PBP2 Δ *gpsB*, ColsGFP-PBP3 Δ *gpsB*,

COLpPBP4-YFP Δ *gpsB*, complemented strains ColsGFP-PBP2 Δ *gpsB* pCNX*gpsB* and COLpPBP4-YFP Δ *gpsB* pCN51*gpsB*, and strains overexpressing *gpsB* ColsGFP-PBP2 pCNX*gpsB* and COLpPBP4-YFP pCN51*gpsB* were grown in TSB 37°C (plus 0.1 μ M CdCl₂ for strains containing pCNX*gpsB* and pCN51*gpsB*) to OD₆₀₀ of 0.5. Images were acquired with the Zeiss Axio Observer Z1 microscope described above, with filters Brightline GFP-3035D and Brightline YFP-2427A (Semrock) to image GFP and YFP derivatives, respectively, with 4,000- to 5,000-ms exposure time.

To evaluate localization of peptidoglycan synthesis activity, *S. aureus* cells of parental strains COL/JE2, *gpsB* mutants COL/JE2 Δ *gpsB*, and complemented strains COL/JE2 Δ *gpsB* pCNX*gpsB* were grown in TSB (plus 0.1 μ M CdCl₂ for the complemented strains) at 37°C, in triplicate, to an OD₆₀₀ of 0.4 and labeled with fluorescent 7-hydroxycoumarin-3-carboxylic acid-amino-D-alanine (HADA) (32) at 0.1 mM for 30 min at 37°C, with agitation. Cells were then washed with PBS and placed on a 1.5% agarose pad mounted on a microscopy slide. Images were acquired with the Zeiss Axio Observer Z1 microscope described above using the filter Brightline DAPI-1160A (Semrock), with 100 ms exposure time.

For image analysis, phase 3 cells (with complete septum) were selected, and the ratio of the fluorescence signal at the septum (considering only the 25% brightest pixels) versus the cell periphery was calculated using eHooke (18). Statistical analysis was performed using a two-sided Mann-Whitney *U* test, performed using the Python package SciPy version 1.10.1 (33).

Bacterial two-hybrid (BTH) assays

Plasmids pUT18-GpsB, pKNT25-GpsB, and pKT25-GpsB were constructed by amplifying by PCR the *gpsB* gene, using primers described in Table S3, and cloning this insert into the BTH plasmids pUT18C, pKNT25, and pKT25. The correct sequence of the insert was confirmed by Sanger sequencing.

Plasmids pUT18 and pKT25 (negative control); p18Zip and p25Zip (positive control); various combinations of constructed plasmids pUT18-GpsB, pKNT25-GpsB, and pKT25-GpsB and plasmids p18PBP2 and p25PBP2 (34) were co-transformed into the reporter strain BTH101 (35). Cells were plated on LB agar supplemented with 40 μ g/mL X-Gal, 0.5 mM IPTG, 100 μ g/mL ampicillin, and 50 μ g/mL kanamycin and incubated for 43 h at 30°C.

Individual colonies from each transformation with a pair of plasmids were resuspended in 10 μ L of LB, and 3 μ L was spotted on MacConkey agar containing 1% maltose, 0.5 mM IPTG, 100 μ g/mL ampicillin, and 50 μ g/mL kanamycin and incubated for 18 h at 30°C. Three independent experiments were conducted.

RESULTS

Screening of NTML for mutants with reduced eccentricity

S. aureus cells undergo minor elongation during the cell cycle (7, 8). To the best of our knowledge, only two proteins, PBP3 and RodA (8), have been identified so far as being required for the elongation process. To identify new determinants required for *S. aureus* elongation, we labeled the 1920 NTML transposon insertion mutants in non-essential genes of JE2 (17), as well as the parental strain JE2, with a membrane dye and a DNA dye and imaged them by fluorescence microscopy. At least five fields of view were imaged for each strain, resulting in a library of over 10,000 images. Morphological parameters of each cell were automatically determined using eHooke software (18), and mutants were ranked from lowest (more spherical) to highest (more elongated) average cell eccentricity.

The top seven mutants with lowest eccentricity were selected for further studies: SAUSA300_1090, *lgt*, *ssaA*, *pbpC* (aka *pbp3*), *rodA*, SAUSA300_0128, and *mreD* (Table S4; Fig. S1). The fact that the third and fourth positions in the ranking of increasing eccentricity were occupied by the genes encoding for RodA and PBP3, required for

elongation (8), validates the screening. Repeating the imaging of selected transposon mutants did not confirm the decreased eccentricity of the *lgt* mutant, which was, therefore, considered a false positive from the screening and not further studied.

From the top 100 hits of the eccentricity screening, we selected two other candidates, GpsB and PknB, which we reasoned could have a role in elongation based on the function of these proteins in other organisms. GpsB contributes to the control of elongation/division in *B. subtilis* by shuttling between the septum and the lateral wall, together with penicillin-binding protein PBP1 (36). In *S. pneumoniae*, depletion of GpsB results in the formation of elongated, enlarged cells, presumably because GpsB mediates septal ring closure (37, 38). Given that the *B. subtilis* serine/threonine kinase PrkC phosphorylates GpsB (39), we also included in our study the main serine/threonine protein kinase present in *S. aureus*, PknB.

Two additional mutants lacking proteins with reported roles in elongation of other bacterial species, MreC and RodZ, were also included in this study. MreC, together with MreD, has a role in cell elongation through the coordination of peripheral peptidoglycan synthesis in *B. subtilis* and *S. pneumoniae* (14, 40). A previous study did not identify morphology changes in *S. aureus* mutants lacking MreD and MreC, but their eccentricity was not determined (21). Given that the *mreD* mutant was a top hit in the screening, we decided to include also the *mreC* mutant in this study, although it ranked lower in the screening (Table S4). RodZ is a non-essential component of the elongosome (also known as Rod complex) of *E. coli* or *B. subtilis*, and *rodZ* deletion results in cell shape changes from rod to round or ovoid (41–43). Although a *rodZ* transposon mutant is absent from the NTML, we were able to generate a *rodZ* deletion mutant in JE2, showing that it is not an essential gene in this *S. aureus* strain.

Finally, we also included the mutant lacking PBP4 because we previously showed that this protein is involved in peripheral peptidoglycan synthesis in *S. aureus* (7). We reasoned that PBP4 could have a role in cell elongation via insertion of peripheral peptidoglycan, despite its low ranking in the screening for cell eccentricity (Table S4).

To confirm the results from the screening and test if the morphology changes in the transposon mutants were not due to polar effects on downstream genes, new mutants were made by individually deleting each selected gene mentioned above from the genome of strain JE2. Furthermore, each deletion mutant was complemented with a plasmid expressing the corresponding gene. Deletion mutants and corresponding complemented strains were labeled with membrane and DNA dyes and imaged by widefield fluorescence microscopy. The eccentricity was measured only in cells with a closed septum (cell cycle phase 3 cells), since elongation is more pronounced in this phase (7, 8) (Fig. 1). As expected, cells of all tested mutants, except for *pbp4*, had lower eccentricity (cells were more spherical) than cells of the parental strains JE2. However, for mutants in *ssaA*, *SAUSA300_0128*, *mreC*, and *mreD*, this phenotype was not fully complemented by the corresponding plasmid-encoded gene, possibly due to the lack of native gene regulation or protein overexpression. The strongest phenotype, which was readily complemented by plasmid-encoded gene, was observed for cells of the *gpsB* deletion mutant, which was, therefore, selected for further studies. Whole genome sequencing of the *gpsB* deletion mutant confirmed the deletion of the gene and identified only one single-nucleotide polymorphism (SNP) leading to a synonymous mutation (G51>T) in the *gatB* gene (*SAUSA300_1880*) encoding aspartyl/glutamyl-tRNA amidotransferase subunit B. We confirmed that deletion of *gpsB* does not impair growth and that the role of GpsB in cell elongation was not unique to JE2, as it was observed in the background of another well-studied MRSA strain, COL (Fig. S2).

Lack of GpsB does not alter FtsZ treadmilling speed

GpsB is a small coiled-coil protein, which localizes at midcell, previously reported to be essential in *S. aureus* strain SH1000 (44). However, a transposon mutant in *gpsB* is present in the NTML (17) and in additional reported transposon screenings (45), and deletion mutants of *gpsB* have been recently reported (46) including in SH1000 (47). We could

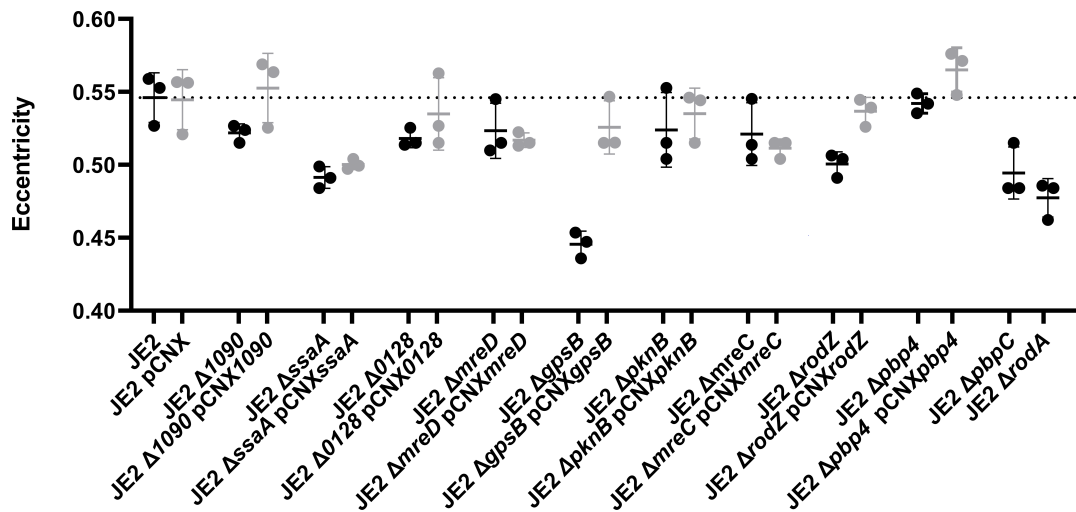


FIG 1 *S. aureus* mutants with reduced eccentricity. Cell eccentricity was measured in cells with a complete septum (cell cycle phase 3, $n = 550$ cells/replicate, three replicates per strain) of selected mutants (black circles). Each mutant was complemented with the corresponding gene encoded in pCNX replicative plasmid (gray circles). The empty vector was introduced in the parental strain JE2. Black and gray lines represent the mean eccentricity and standard deviation of the three replicates of each strain. The average eccentricity of JE2 cells is indicated by the dashed line.

also easily delete *gpsB* from both COL and JE2 strains, indicating that *gpsB* is dispensable for growth in various *S. aureus* strains. The function of GpsB in *S. aureus* is still not fully elucidated, but it has been proposed to promote stabilization of the Z-ring at the onset of cell division (although in a mutant that required GpsB for growth [44]). This was suggested to result in higher local concentration of FtsZ, activation of its GTPase activity, and triggering of FtsZ treadmilling (44). In *S. aureus*, FtsZ treadmilling is essential during the early stages of cytokinesis (24). We hypothesized that regulation of FtsZ treadmilling activity by GpsB could modulate peptidoglycan synthesis at the septum, causing the morphology changes observed in the *gpsB* mutant. To measure FtsZ treadmilling speed, we used as a proxy a functional fusion of superfast GFP (sGFP) (48) to EzrA, a direct interaction partner of FtsZ. We have previously shown that FtsZ and EzrA undergo similar movement dynamics, sensitive to FtsZ inhibitor PC190723 (24). Our quantitative analysis focused on the early stages of cytokinesis, in which nascent Z-rings appear sparse and Dshaped, in newborn sister cells that are still attached via the septum of the mother cell (Fig. 2a), given that GpsB was proposed to stabilize FtsZ at the onset of cell division (44). We observed that in TSB-rich medium at 37°C, FtsZ filaments/bundles moved at the same speed in the parental strain COL EzrA-sGFP (57.7 ± 7.8 nm/s; $n = 130$) and the *gpsB* deletion mutant COL EzrA-sGFP Δ *gpsB* (58.7 ± 8.9 nm/s; $n = 132$) (Fig. 2b), indicating that GpsB does not affect FtsZ treadmilling. Therefore, *S. aureus* cell morphology changes in the *gpsB* mutant are not mediated by regulation of FtsZ treadmilling.

PBP2 and PBP4 partially delocalize from the septum in the absence of GpsB

Besides interacting with FtsZ (44), *S. aureus* GpsB also interacts with PBP4 through a signature GpsB recognition sequence, suggesting that it may link cell division and peptidoglycan synthesis (49, 50). If correct localization of one or more *S. aureus* PBPs was dependent on GpsB, then its absence could result in peptidoglycan incorporation at incorrect cellular locations, which could lead to morphological alterations. To test if this was the case, we deleted *gpsB* in four previously constructed strains expressing fluorescent fusions to each of the four *S. aureus* native PBPs, PBP1–4, and imaged the resulting strains by fluorescence microscopy. PBP1, an essential class b PBP with transpeptidase activity, was previously shown to localize at the septum. This localization was not altered in the absence of GpsB, as the sGFP-PBP1 fluorescence signal was present at the septum and absent from the peripheral membrane in both ColsGFP-PBP1 and ColsGFP-PBP1

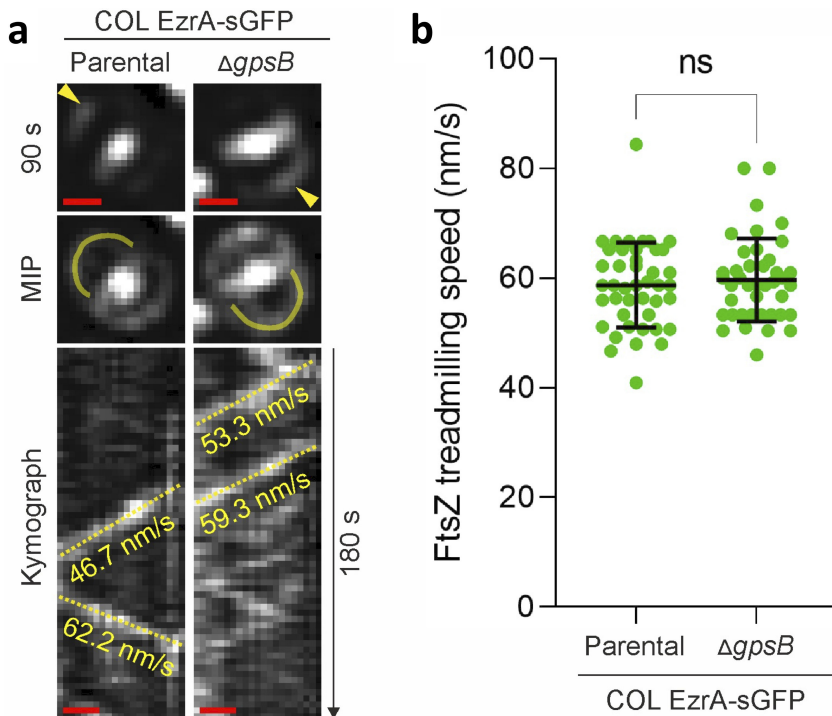


FIG 2 GpsB does not affect FtsZ treadmilling speed *in vivo*. (a) Representative epifluorescence images of EzrA-sGFP in pre-divisional cells with nascent Z-rings of strains COL EzrA-sGFP (parental) and COL EzrA-sGFP Δ *gpsB* at a selected time point and throughout a 180-second time series (MIP, maximum intensity projection). Representative cells with nascent Z-rings are shown for each strain. Yellow arrow heads indicate an EzrA-sGFP patch whose change in localization was followed over time. Kymographs were generated by extracting fluorescence intensity values along indicated yellow lines. Yellow dashed lines in kymographs indicate the slopes used to calculate EzrA-sGFP movement speed (in nanometers per second), a proxy for FtsZ treadmilling. Scale bars, 0.5 μ m. (b) FtsZ treadmilling speed measured in indicated strains. Data are represented as scatter plots in which the middle line represents the mean, and the top and bottom lines show the standard deviation of slopes determined from diagonal lines in kymographs. Experiments were performed in triplicate. Statistical analysis was performed using a two-tailed Mann-Whitney *U* test ($P = 0.5179$); COL EzrA-sGFP, $n_{\text{total}} = 130$. COL EzrA-sGFP Δ *gpsB*, $n_{\text{total}} = 132$; ns, non-significant.

Δ *gpsB* (Fig. 3a). For strains expressing fluorescent derivatives of PBP2, 3, and 4 (which are enriched at the septum but also present at the cell periphery), we calculated the ratio of the fluorescence signal at the septum versus the cell periphery (FR, Fig. 3b). PBP3 showed very mild, if any, delocalization, while FR for both PBP2 and PBP4 decreased in the absence of GpsB, indicating partial delocalization of these proteins from the septum to the cell periphery. PBP2 is the only bifunctional PBP in *S. aureus*, with both glycosyltransferase and transpeptidase activity, for synthesis of the glycan strands and crosslinking via peptide bridges, respectively (51). PBP4 is a low-molecular-weight PBP with transpeptidase activity, responsible for the high levels of crosslinking characteristic of *S. aureus*, shown to be involved in peptidoglycan synthesis at the cell periphery (7, 52). To confirm that PBP2 and PBP4 partial delocalization from the septum was in fact caused by lack of GpsB, we complemented strains COLsGFP-PBP2 Δ *gpsB* and COLpPBP4-YFP Δ *gpsB* with plasmid-encoded *gpsB*, and in both cases, septal enrichment was recovered (Fig. 3b). PBP2 septal enrichment was further increased upon overexpression of GpsB, although we could not observe the same for PBP4 (Fig. 3b). However, the importance of PBP4 peripheral activity for the decreased eccentricity of cells lacking GpsB is clear, as deleting both *pbp4* and *gpsB* results in cells with eccentricity similar to those of the parental strain COL (Fig. S3).

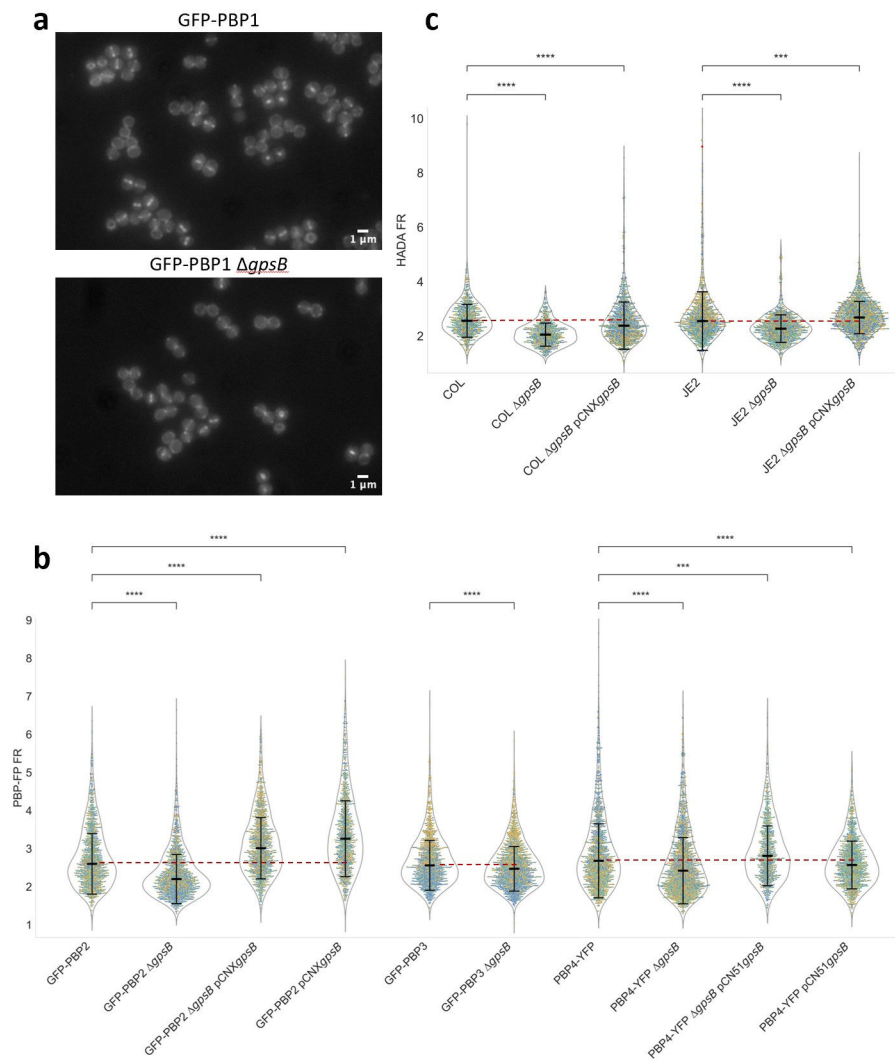


FIG 3 PBP2 and PBP4 partially delocalize from the septum in the absence of GpsB, leading to increased peptidoglycan synthesis at the cell periphery versus the septum. Strains ColsGFP-PBP1, BCpM073 (encoding sGFP-PBP2), ColsGFP-PBP3, and COLpPBP4-YFP, expressing fluorescent derivatives of the four *S. aureus* native PBPs, the corresponding *gpsB* deletion mutants, the GpsB-complemented strains ColsGFP-PBP2 Δ *gpsB* pCNX*gpsB* and COLpPBP4-YFP Δ *gpsB* pCN51*gpsB*, and GpsB-overexpressing strains ColsGFP-PBP2 pCNX*gpsB* and COLpPBP4-YFP pCN51*gpsB* were imaged by fluorescence microscopy. (a) No change was observed in the localization pattern of the fluorescent derivatives of PBP1 in the absence of GpsB, with PBP1 localizing exclusively at the septum in ColsGFP-PBP1 and the corresponding *gpsB* deletion mutant. (b) PBP2 and PBP4 partially delocalized from the division septum in the absence of GpsB, while PBP3 showed very mild, if any, delocalization. PBP2 and PBP4 delocalization in the *gpsB* mutants is reverted upon complementation with plasmid encoded *gpsB*. PBP2 (but not PBP4) septal enrichment is further increased upon overexpression of GpsB. Graph shows the ratio of the signal of fluorescent derivatives of PBPs at the septum versus the peripheral membrane (PBP:FP:FR), in cells with a complete septum. (c) Parental strains COL/JE2, *gpsB* mutants COL/JE2 Δ *gpsB*, and complemented strains COL/JE2 Δ *gpsB* pCNX*gpsB* cells were labeled for 30 min with HADA, a fluorescent derivative of D-alanine that is incorporated in peptidoglycan. Graph shows the ratio of the fluorescent signal of HADA at the septum versus the peripheral membrane (HADA:FR), in cells with a complete septum. This ratio is lower for *gpsB* mutants indicating that there is higher peptidoglycan synthesis activity at the cell periphery versus the septum in the absence of GpsB, and reverts to levels close to those observed in the parental strains upon complementation with plasmid encoded *gpsB*. (b and c) Strains containing pCNX*gpsB* and pCN51*gpsB* were grown in the presence of 0.1 μ M CdCl₂ to induce *gpsB* expression. Experiments were done in triplicate with yellow, green, and blue dots corresponding to each replicate ($n_{\text{total}} > 1,150$ for GFP-PBP2 samples, $n_{\text{total}} > 1,300$ for GFP-PBP3 samples, $n_{\text{total}} > 975$ for PBP4-YFP samples; in graph 3c, $n_{\text{total}} > 730$ for COL strains and $n_{\text{total}} > 1,065$ for JE2 strains). Black lines show medians and standard deviations. Red dashed line indicates FR mean of parental strains to facilitate comparison with mutants. Statistical analysis was performed using a two-sided Mann-Whitney *U* test; **** $0.0001 < P < 0.001$, ***** $P < 0.0001$.

As mentioned above, PBP4 has been shown to interact with GpsB (49). However, to the best of our knowledge, this has not been shown for PBP2. We, therefore, tested, by bacterial two-hybrid assay, if we could detect an interaction between PBP2 and GpsB (Fig. 4). Our data confirm that GpsB and PBP2 self-interact, as previously shown (49, 53), and suggest that GpsB interacts with PBP2, although this protein lacks a GpsB recognition motif (49). Therefore, the role of GpsB in the regulation of PBP2 and PBP4 localization may be mediated by protein-protein interactions.

Partial delocalization of PBP2 and PBP4 to the cell periphery should lead to increased peptidoglycan synthesis over the entire cell surface. We labeled strains COL and JE2 as well as the corresponding COL/JE2 Δ *gpsB* mutants and COL/JE2 Δ *gpsB* pCNX*gpsB* complemented strains, with HADA, a fluorescent derivative of D-alanine which is specifically incorporated into the pentapeptide chain of peptidoglycan (32). We observed that the ratio between peptidoglycan synthesis at the septum versus the cell periphery decreases in the absence of GpsB, a phenotype that is reversed in the complemented strains (Fig. 3c). This increased peripheral synthesis may increase the stiffness of the peripheral wall and/or override the RodA/PBP3-mediated synthesis at the outer edge of the septum, previously shown to be required for *S. aureus* elongation (8), resulting in rounder cells in the *gpsB* mutants.

DISCUSSION

Elongation of *S. aureus* is dispensable *in vitro*, as mutants lacking the RodA/PBP3 pair of peptidoglycan synthases, required for elongation, exhibit no growth defects in laboratory conditions such as TSB-rich medium and 37°C (8). However, the retention of an (albeit minor) elongation capacity throughout evolution implies potential advantages in alternative conditions. Interestingly, in a murine model of osteomyelitis, an infection primarily caused by *S. aureus*, staphylococcal cells were observed as submicron rod-shaped bacteria within the canaliculi of live cortical bone (54). This suggests that deformation/elongation of *S. aureus* may be required for migration in bones during

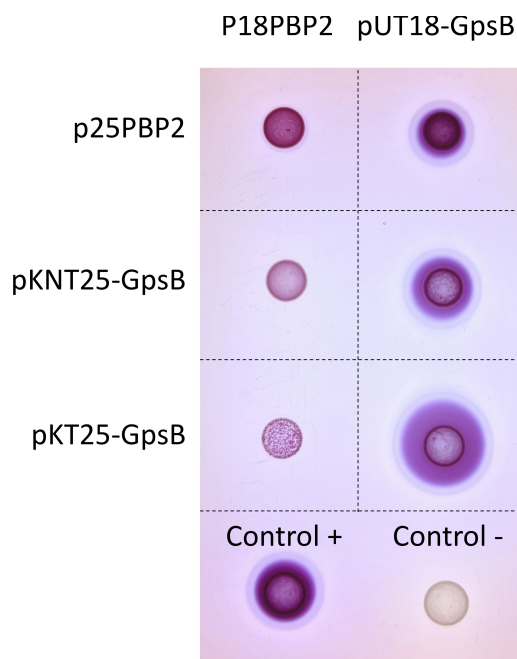


FIG 4 GpsB and PBP2 interact in a bacterial two-hybrid assay. A bacterial two-hybrid assay detected self-interaction of PBP2 and GpsB, as well as an interaction between PBP2 and GpsB. Plasmids p18Zip and p25Zip were used as a positive control, and empty vectors pUT18C and pKT25 were used as negative control. *E. coli* BTH101 strains containing pairs of plasmids indicated in the figure were spotted in maltose-containing MacConkey where red color indicates an interaction.

osteomyelitis (54). Furthermore, while wild-type USA300 *S. aureus* cells were capable of propagation through a nanopore narrower than the diameter of the cells, mutants lacking PBP3 or PBP4 showed reduced propagation through the nanopores, suggesting impaired ability to undergo the required deformation (55, 56). These mutants also failed to invade and colonize the canaliculi of cortical bone (55, 56), indicating that the ability to deform/elongate is required during osteomyelitis. Therefore, understanding the mechanism of elongation of *S. aureus* may be relevant not only for expanding our knowledge of cocci morphogenesis, but also to gain a better understanding of how this bacterial pathogen causes an infection that is often regarded as incurable (54).

In this work, we analyzed the impact of individually deleting 11 non-essential genes on the eccentricity of *S. aureus* cells. Two of these genes encoded RodA and PBP3, the SEDS/PBP pair previously reported to be involved in *S. aureus* elongation (8). The remaining nine mutants all had decreased eccentricity, indicating that elongation of *S. aureus* may be a complex process requiring multiple determinants. However, the phenotype of five of these mutants was very mild: two mutants lacking proteins of unknown function (SAUSA300_1090 and SAUSA300_0128) and three mutants lacking MreC or MreD, two proteins with a well-studied role in elongation of rods (14, 57), and the serine/threonine protein kinase PknB (Fig. 1). In agreement with its low ranking in the initial NLTM screening for altered eccentricity, the mutant lacking PBP4, a peptidoglycan transpeptidase involved in peripheral peptidoglycan synthesis in *S. aureus* (7), showed similar eccentricity to that of the parental strain JE2 (Fig. 1). The remaining three mutants showed a stronger phenotype, with eccentricity being reduced by close to 10%. These include mutants lacking (i) RodZ, a member of the elongasome of rods in which it interacts with MreC, MreD, and RodA/bPBPs, possibly modulating MreB filament density in *B. subtilis* (16) and linking MreB filaments to the elongation peptidoglycan synthases (15). RodZ is also present in ovococoid bacteria such as *S. pneumoniae*, where it seems to act as a scaffold protein of the elongasome despite the absence of MreB (58), a role that may be similar to its role in *S. aureus*; (ii) SsaA, an autolysin with amidase activity (59). For peptidoglycan to expand in surface area, a process presumably required for cell elongation, both synthesis and hydrolysis are required to allow for insertion of new material and relaxation of old material. SsaA may have a role in the relaxation of the peptidoglycan mesh at midcell during elongation, but further studies are required to test this hypothesis; (iii) GpsB, a small membrane associated protein, is widely conserved in firmicutes and proposed to coordinate peptidoglycan synthesis for cell growth and division by binding cytoplasmic mini-domains of PBPs to ensure their correct subcellular localization (50). In *S. pneumoniae*, which lacks MreB, similarly to *S. aureus*, GpsB is part of a molecular switch that orchestrates peripheral and septal peptidoglycan synthesis, and cells elongate in the absence of GpsB (37, 38). The *S. aureus* mutant lacking GpsB was the only one in this study with cells more spherical (lower eccentricity) than those of the RodA/PBP3 mutants, pointing to an important role of this protein in staphylococcal morphogenesis. We, therefore, focused on understanding the mechanism by which GpsB regulates cell shape in *S. aureus*. Interestingly, data concurrent with ours show that *gpsB* deletion in *S. aureus* SH1000 also results in more spherical cells (47).

GpsB was previously suggested to regulate FtsZ treadmilling in *S. aureus* (44), which could alter peptidoglycan synthesis activity at the septum. However, we did not see any change in FtsZ treadmilling speed upon deletion of *gpsB*. Alternatively, given that GpsB was recently shown to interact with PBP4 in *S. aureus* (49), we hypothesized that GpsB could modulate *S. aureus* cell shape by directing PBPs to the cell periphery or to the septum. In agreement with this hypothesis, we observed that both PBP2 (which we showed also interacts with GpsB) and PBP4 partially delocalize from the septum to the peripheral wall in the absence of GpsB. This results in higher peptidoglycan synthesis activity in the cell periphery, which was confirmed by increased incorporation of the fluorescent D-amino acid HADA in the peptidoglycan of the peripheral wall versus the septum. Localized peptidoglycan synthesis at the sidewall of the septal region is required for cell elongation in *S. aureus* (8). We propose that the increased peptidoglycan

synthesis at the cell periphery in the absence of GpsB overrides the localized RodA/PBP3-mediated peptidoglycan synthesis at midcell, leading to more spherical cells. Conversely, in wild-type cells that express GpsB, PBP2 and PBP4 activity is more restricted to the septum, and expansion of the peripheral wall occurs mostly near the outer edge of the septum, allowing mild elongation of *S. aureus* cells. It is also possible that increased peripheral activity of PBP2 and PBP4 in a *gpsB* mutant and the consequent increase in peptidoglycan crosslinking lead to a stiffer peripheral wall that does not expand to elongate, resulting in rounder and smaller cells in the absence GpsB.

Our data do not necessarily imply that GpsB is a member of an elongasome complex but that it has a role in ensuring correct morphogenesis of *S. aureus* by contributing to the spatio-temporal regulation of PBPs.

ACKNOWLEDGMENTS

We thank Zach Hensel (ITQB-NOVA) and Ludwig Krippahl (FCT-NOVA) for helpful discussions and Mike VanNieuwenhze (Indiana University) for the generous gift of HADA.

This study was funded by the European Research Council through grant ERC-2017-CoG-771709 (to M.G.P.); by national funds from FCT-Fundação para a Ciência e a Tecnologia through PTDC/BIA-MIC/6982/2020 (to H.V.), MOSTMICRO-ITQB R&D Unit (UIDB/04612/2020, UIDP/04612/2020 to ITQB-NOVA), and LS4FUTURE Associated Laboratory (LA/P/0087/2020 to ITQB-NOVA); by contract 2022.03033.CEECIND (to S.S.), fellowships PD/BD/135480/2018 (to S.F.C.), COVID/BD/152499/2022 (to S.F.C.), SFRH/BD/147052/2019 (to B.M.S.), UI/BD/153384/2022 (to L.B.M.), SFRH/BD/143461/2019 (to A.M.D.), and 2021.06849.BD (to A.D.B.); and by the European Union's Horizon 2020 research and innovation program under the Marie Skłodowska-Curie grant agreement no. 839596 (to S.S.).

AUTHOR AFFILIATION

¹Instituto de Tecnologia Química e Biológica António Xavier, Universidade NOVA de Lisboa, Oeiras, Portugal

AUTHOR ORCIDs

Bruno M. Saraiva <http://orcid.org/0000-0002-9151-5477>
 Helena Veiga <http://orcid.org/0000-0001-5345-475X>
 Leonor B. Marques <http://orcid.org/0009-0004-8243-9195>
 Simon Schäper <http://orcid.org/0000-0003-3760-9541>
 António D. Brito <http://orcid.org/0009-0001-1769-2627>
 Patricia Reed <http://orcid.org/0000-0002-4263-6993>
 Mariana G. Pinho <http://orcid.org/0000-0002-7132-8842>

FUNDING

Funder	Grant(s)	Author(s)
EC European Research Council (ERC)	2017-CoG-771709	Mariana G. Pinho
MEC Fundação para a Ciência e a Tecnologia (FCT)	PTDC/BIA-MIC/6982/2020	Helena Veiga

AUTHOR CONTRIBUTIONS

Sara F. Costa, Conceptualization, Investigation, Methodology, Writing – original draft, Writing – review and editing, Formal analysis | Bruno M. Saraiva, Conceptualization, Formal analysis, Investigation, Methodology, Software, Writing – review and editing | Helena Veiga, Formal analysis, Investigation, Writing – review and editing | Leonor B. Marques, Formal analysis, Investigation, Writing – review and editing | Simon Schäper, Formal analysis, Investigation, Writing – review and editing | Marta Sporniak,

Investigation | Daniel E. Vega, Investigation | Ana M. Jorge, Investigation, Resources | Andreia M. Duarte, Investigation, Writing – review and editing | António D. Brito, Formal analysis, Software, Writing – review and editing | Andreia C. Tavares, Investigation, Writing – review and editing | Patricia Reed, Resources | Mariana G. Pinho, Conceptualization, Funding acquisition, Methodology, Project administration, Supervision, Writing – original draft, Writing – review and editing

DATA AVAILABILITY

Data will be made available upon reasonable request to the corresponding author.

ADDITIONAL FILES

The following material is available [online](#).

Supplemental Material

Supplemental material (mBio03235-23-s0001.docx). Supplemental tables and figures.

REFERENCES

- Murray CJL, Ikuta KS, Sharara F, Swetschinski L, Robles Aguilar G, Gray A, Han C, Bisignano C, Rao P, Wool E, et al. 2022. Global burden of bacterial antimicrobial resistance in 2019: a systematic analysis. *The Lancet* 399:629–655. [https://doi.org/10.1016/S0140-6736\(21\)02724-0](https://doi.org/10.1016/S0140-6736(21)02724-0)
- van Teeffelen S, Renner LD. 2018. Recent advances in understanding how rod-like bacteria stably maintain their cell shapes. *F1000Res* 7:241. <https://doi.org/10.12688/f1000research.12663.1>
- den Blaauwen T, Hamoen LW, Levin PA. 2017. The divisome at 25: the road ahead. *Curr Opin Microbiol* 36:85–94. <https://doi.org/10.1016/j.mib.2017.01.007>
- Chastanet A, Carballido-Lopez R. 2012. The actin-like MreB proteins in *Bacillus subtilis*: a new turn. *Front Biosci (Schol Ed)* 4:1582–1606. <https://doi.org/10.2741/s354>
- Pinho MG, Kjos M, Veening J-W. 2013. How to get (a)round: mechanisms controlling growth and division of coccoid bacteria. *Nat Rev Microbiol* 11:601–614. <https://doi.org/10.1038/nrmicro3088>
- Lleo MM, Caneparì P, Satta G. 1990. Bacterial cell shape regulation: testing of additional predictions unique to the two-competing-sites model for peptidoglycan assembly and isolation of conditional rod-shaped mutants from some wild-type cocci. *J Bacteriol* 172:3758–3771. <https://doi.org/10.1128/jb.172.7.3758-3771.1990>
- Monteiro JM, Fernandes PB, Vaz F, Pereira AR, Tavares AC, Ferreira MT, Pereira PM, Veiga H, Kuru E, VanNieuwenhze MS, Brun YV, Filipe SR, Pinho MG. 2015. Cell shape dynamics during the staphylococcal cell cycle. *Nat Commun* 6:8055. <https://doi.org/10.1038/ncomms9055>
- Reichmann NT, Tavares AC, Saraiva BM, Jouselin A, Reed P, Pereira AR, Monteiro JM, Sobral RG, VanNieuwenhze MS, Fernandes F, Pinho MG. 2019. SEDS-bPBP pairs direct lateral and septal peptidoglycan synthesis in *Staphylococcus aureus*. *Nat Microbiol* 4:1368–1377. <https://doi.org/10.1038/s41564-019-0437-2>
- Sham L-T, Tsui H-C, Land AD, Barendt SM, Winkler ME. 2012. Recent advances in pneumococcal peptidoglycan biosynthesis suggest new vaccine and antimicrobial targets. *Curr Opin Microbiol* 15:194–203. <https://doi.org/10.1016/j.mib.2011.12.013>
- Trouve J, Zapun A, Arthaud C, Durmort C, Di Guilmi AM, Söderström B, Pelletier A, Grangeasse C, Bourgeois D, Wong Y-S, Morlot C. 2021. Nanoscale dynamics of peptidoglycan assembly during the cell cycle of *Streptococcus pneumoniae*. *Curr Biol* 31:2844–2856. <https://doi.org/10.1016/j.cub.2021.04.041>
- van Teeffelen S, Wang S, Furchtgott L, Huang KC, Wingreen NS, Shaevitz JW, Gitai Z. 2011. The bacterial actin MreB rotates, and rotation depends on cell-wall assembly. *Proc Natl Acad Sci U S A* 108:15822–15827. <https://doi.org/10.1073/pnas.1108999108>
- Dominguez-Escobar J, Chastanet A, Crevenna AH, Fromion V, Wedlich-Söldner R, Carballido-López R. 2011. Processive movement of MreB-associated cell wall biosynthetic complexes in bacteria. *Science* 333:225–228. <https://doi.org/10.1126/science.1203466>
- Garner EC, Bernard R, Wang W, Zhuang X, Rudner DZ, Mitchison T. 2011. Coupled, circumferential motions of the cell wall synthesis machinery and MreB filaments in *B. subtilis*. *Science* 333:222–225. <https://doi.org/10.1126/science.1203285>
- Leaver M, Errington J. 2005. Roles for MreC and MreD proteins in helical growth of the cylindrical cell wall in *Bacillus subtilis*. *Mol Microbiol* 57:1196–1209. <https://doi.org/10.1111/j.1365-2958.2005.04736.x>
- Ago R, Shiomi D. 2019. RodZ: a key-player in cell elongation and cell division in *Escherichia coli*. *AIMS Microbiol* 5:358–367. <https://doi.org/10.3934/microbiol.2019.4.358>
- Sun Y, Hürlimann S, Garner E. 2023. Growth rate is modulated by monitoring cell wall precursors in *Bacillus subtilis*. *Nat Microbiol* 8:469–480. <https://doi.org/10.1038/s41564-023-01329-7>
- Fey PD, Endres JL, Yajjala VK, Widhelm TJ, Boissy RJ, Bose JL, Bayles KW. 2013. A genetic resource for rapid and comprehensive phenotype screening of nonessential *Staphylococcus aureus* genes. *mBio* 4:e00537-12. <https://doi.org/10.1128/mBio.00537-12>
- Saraiva BM, Krippahl L, Filipe SR, Henriques R, Pinho MG. 2021. eHooke: a tool for automated image analysis of spherical bacteria based on cell cycle progression. *Biol Imaging* 1:e3. <https://doi.org/10.1017/S2633903X21000027>
- Arnaud M, Chastanet A, Débarbouillé M. 2004. New vector for efficient allelic replacement in naturally nontransformable, low-GC-content, gram-positive bacteria. *Appl Environ Microbiol* 70:6887–6891. <https://doi.org/10.1128/AEM.70.11.6887-6891.2004>
- Gibson DG, Young L, Chuang R-Y, Venter JC, Hutchison CA, Smith HO. 2009. Enzymatic assembly of DNA molecules up to several hundred kilobases. *Nat Methods* 6:343–345. <https://doi.org/10.1038/nmeth.1318>
- Tavares AC, Fernandes PB, Carballido-López R, Pinho MG. 2015. MreC and MreD proteins are not required for growth of *Staphylococcus aureus*. *PLoS One* 10:e0140523. <https://doi.org/10.1371/journal.pone.0140523>
- Veiga H, Pinho MG. 2009. Inactivation of the Saul type I restriction-modification system is not sufficient to generate *Staphylococcus aureus* strains capable of efficiently accepting foreign DNA. *Appl Environ Microbiol* 75:3034–3038. <https://doi.org/10.1128/AEM.01862-08>
- Oshida T, Tomasz A. 1992. Isolation and characterization of a Tn551-autolysis mutant of *Staphylococcus aureus*. *J Bacteriol* 174:4952–4959. <https://doi.org/10.1128/jb.174.15.4952-4959.1992>
- Monteiro JM, Pereira AR, Reichmann NT, Saraiva BM, Fernandes PB, Veiga H, Tavares AC, Santos M, Ferreira MT, Macário V, VanNieuwenhze MS, Filipe SR, Pinho MG. 2018. Peptidoglycan synthesis drives an FtsZ-treadmilling-independent step of cytokinesis. *Nature* 554:528–532. <https://doi.org/10.1038/nature25506>
- Tan CM, Therien AG, Lu J, Lee SH, Caron A, Gill CJ, Lebeau-Jacob C, Benton-Perdomo L, Monteiro JM, Pereira PM, et al. 2012. Restoring methicillin-resistant *Staphylococcus aureus* susceptibility to β -lactam

- antibiotics. *Sci Transl Med* 4:126ra35. <https://doi.org/10.1126/scitranslmed.3003592>
26. Loskill P, Pereira PM, Jung P, Bischoff M, Herrmann M, Pinho MG, Jacobs K. 2014. Reduction of the peptidoglycan crosslinking causes a decrease in stiffness of the *Staphylococcus aureus* cell envelope. *Biophys J* 107:1082–1089. <https://doi.org/10.1016/j.bpj.2014.07.029>
 27. Saraiva BM, Sorg M, Pereira AR, Ferreira MJ, Caulat LC, Reichmann NT, Pinho MG. 2020. Reassessment of the distinctive geometry of *Staphylococcus aureus* cell division. *Nat Commun* 11:4097. <https://doi.org/10.1038/s41467-020-17940-9>
 28. Charpentier E, Anton Al, Barry P, Alfonso B, Fang Y, Novick RP. 2004. Novel cassette-based shuttle vector system for gram-positive bacteria. *Appl Environ Microbiol* 70:6076–6085. <https://doi.org/10.1128/AEM.70.10.6076-6085.2004>
 29. Laine RF, Tosheva KL, Gustafsson N, Gray RDM, Almada P, Albrecht D, Risa GT, Hurtig F, Lindås A-C, Baum B, Mercer J, Leterrier C, Pereira PM, Culley S, Henriques R. 2019. NanoJ: a high-performance open-source super-resolution microscopy toolbox. *J Phys D Appl Phys* 52:163001. <https://doi.org/10.1088/1361-6463/ab0261>
 30. Schindelin J, Arganda-Carreras I, Frise E, Kaynig V, Longair M, Pietzsch T, Preibisch S, Rueden C, Saalfeld S, Schmid B, Tinevez JY, White DJ, Hartenstein V, Eliceiri K, Tomancak P, Cardona A. 2012. Fiji: an open-source platform for biological-image analysis. *Nat Methods* 9:676–682. <https://doi.org/10.1038/nmeth.2019>
 31. Rueden CT, Schindelin J, Hiner MC, DeZonia BE, Walter AE, Arena ET, Eliceiri KW. 2017. ImageJ2: ImageJ for the next generation of scientific image data. *BMC Bioinformatics* 18:529. <https://doi.org/10.1186/s12859-017-1934-z>
 32. Kuru E, Hughes HV, Brown PJ, Hall E, Tekkam S, Cava F, de Pedro MA, Brun YV, VanNieuwenhze MS. 2012. *In situ* probing of newly synthesized peptidoglycan in live bacteria with fluorescent D-amino acids. *Angew Chem Int Ed Engl* 51:12519–12523. <https://doi.org/10.1002/anie.201206749>
 33. Virtanen P, Gommers R, Oliphant TE, Haberland M, Reddy T, Cournapeau D, Burovski E, Peterson P, Weckesser W, Bright J, et al. 2020. SciPy 1.0: fundamental algorithms for scientific computing in Python. *Nat Methods* 17:261–272. <https://doi.org/10.1038/s41592-020-0772-5>
 34. Reed P, Veiga H, Jorge AM, Terrak M, Pinho MG. 2011. Monofunctional transglycosylases are not essential for *Staphylococcus aureus* cell wall synthesis. *J Bacteriol* 193:2549–2556. <https://doi.org/10.1128/JB.01474-10>
 35. Karimova G, Pidoux J, Ullmann A, Ladant D. 1998. A bacterial two-hybrid system based on a reconstituted signal transduction pathway. *Proc Natl Acad Sci U S A* 95:5752–5756. <https://doi.org/10.1073/pnas.95.10.5752>
 36. Claessen D, Emmins R, Hamoen LW, Daniel RA, Errington J, Edwards DH. 2008. Control of the cell elongation-division cycle by shuttling of PBP1 protein in *Bacillus subtilis*. *Mol Microbiol* 68:1029–1046. <https://doi.org/10.1111/j.1365-2958.2008.06210.x>
 37. Land AD, Tsui H-C, Kocaoglu O, Vella SA, Shaw SL, Keen SK, Sham L-T, Carlson EE, Winkler ME. 2013. Requirement of essential Pbp2x and GpsB for septal ring closure in *Streptococcus pneumoniae* D39. *Mol Microbiol* 90:939–955. <https://doi.org/10.1111/mmi.12408>
 38. Fleurie A, Manuse S, Zhao C, Campo N, Cluzel C, Lavergne J-P, Fretton C, Combet C, Guiral S, Soufi B, Macek B, Kuru E, VanNieuwenhze MS, Brun YV, Di Guilmi A-M, Claverys J-P, Galinier A, Grangeasse C. 2014. Interplay of the serine/threonine-kinase StkP and the paralogs DivIVA and GpsB in pneumococcal cell elongation and division. *PLoS Genet* 10:e1004275. <https://doi.org/10.1371/journal.pgen.1004275>
 39. Pompeo F, Foulquier E, Serrano B, Grangeasse C, Galinier A. 2015. Phosphorylation of the cell division protein GpsB regulates PrkC kinase activity through a negative feedback loop in *Bacillus subtilis*. *Mol Microbiol* 97:139–150. <https://doi.org/10.1111/mmi.13015>
 40. Land AD, Winkler ME. 2011. The requirement for pneumococcal MreC and MreD is relieved by inactivation of the gene encoding PBP1a. *J Bacteriol* 193:4166–4179. <https://doi.org/10.1128/JB.05245-11>
 41. Alyahya SA, Alexander R, Costa T, Henriques AO, Emonet T, Jacobs-Wagner C. 2009. RodZ, a component of the bacterial core morphogenic apparatus. *Proc Natl Acad Sci U S A* 106:1239–1244. <https://doi.org/10.1073/pnas.0810794106>
 42. Bendezú FO, Hale CA, Bernhardt TG, de Boer PAJ. 2009. RodZ (YfgA) is required for proper assembly of the MreB actin cytoskeleton and cell shape in *E. coli*. *EMBO J* 28:193–204. <https://doi.org/10.1038/emboj.2008.264>
 43. Muchová K, Chromiková Z, Barák I. 2013. Control of *Bacillus subtilis* cell shape by RodZ. *Environ Microbiol* 15:3259–3271. <https://doi.org/10.1111/1462-2920.12200>
 44. Eswara PJ, Brzozowski RS, Viola MG, Graham G, Spanoudis C, Trebino C, Jha J, Aubee JI, Thompson KM, Camberg JL, Ramamurthi KS. 2018. An essential *Staphylococcus aureus* cell division protein directly regulates FtsZ dynamics. *Elife* 7:e38856. <https://doi.org/10.7554/eLife.38856>
 45. Pang T, Wang X, Lim HC, Bernhardt TG, Rudner DZ. 2017. The nucleoid occlusion factor Noc controls DNA replication initiation in *Staphylococcus aureus*. *PLoS Genet* 13:e1006908. <https://doi.org/10.1371/journal.pgen.1006908>
 46. Bartlett TM, Sisley TA, Mychack A, Walker S, Baker RW, Rudner DZ, Bernhardt TG. 2023. Identification of FacZ as a division site placement factor in *Staphylococcus aureus*. *bioRxiv:2023.04.24.538170*. <https://doi.org/10.1101/2023.04.24.538170>
 47. Sutton JAF, Cooke M, Tinajero-Trejo M, Wacnik K, Salamaga B, Portman-Ross C, Lund VA, Hobbs JK, Foster SJ. 2023. The roles of GpsB and DivIVA in *Staphylococcus aureus* growth and division. *Front Microbiol* 14:1241249. <https://doi.org/10.3389/fmicb.2023.1241249>
 48. Fisher AC, DeLisa MP. 2008. Laboratory evolution of fast-folding green fluorescent protein using secretory pathway quality control. *PLoS ONE* 3:e2351. <https://doi.org/10.1371/journal.pone.0002351>
 49. Sacco MD, Hammond LR, Noor RE, Bhattacharya D, Madsen JJ, Zhang X, Butler SG, Kemp MT, Jaskolka-Brown AC, Khan SJ, Gelis I, Eswara PJ, Chen Y. 2022. *Staphylococcus aureus* FtsZ and PBP4 bind to the conformationally dynamic N-terminal domain of GpsB. *bioRxiv*. <https://doi.org/10.1101/2022.10.25.513704>
 50. Cleverley RM, Rutter ZJ, Rismondo J, Corona F, Tsui H-C, Alatawi FA, Daniel RA, Halbedel S, Massidda O, Winkler ME, Lewis RJ. 2019. The cell cycle regulator GpsB functions as cytosolic adaptor for multiple cell wall enzymes. *Nat Commun* 10:261. <https://doi.org/10.1038/s41467-018-08056-2>
 51. Pinho MG, de Lencastre H, Tomasz A. 2001. An acquired and a native penicillin-binding protein cooperate in building the cell wall of drug-resistant staphylococci. *Proc Natl Acad Sci U S A* 98:10886–10891. <https://doi.org/10.1073/pnas.191260798>
 52. Memmi G, Filipe SR, Pinho MG, Fu Z, Cheung A. 2008. *Staphylococcus aureus* PBP4 is essential for β -lactam resistance in community-acquired methicillin-resistant strains. *Antimicrob Agents Chemother* 52:3955–3966. <https://doi.org/10.1128/AAC.00049-08>
 53. Steele VR, Bottomley AL, Garcia-Lara J, Kasturiarachchi J, Foster SJ. 2011. Multiple essential roles for EzrA in cell division of *Staphylococcus aureus*. *Mol Microbiol* 80:542–555. <https://doi.org/10.1111/j.1365-2958.2011.07591.x>
 54. de Mesy Bentley KL, Trombetta R, Nishitani K, Bello-Irizarry SN, Ninomiya M, Zhang L, Chung HL, McGrath JL, Daiss JL, Awad HA, Kates SL, Schwarz EM. 2017. Evidence of *Staphylococcus aureus* deformation, proliferation, and migration in canaliculi of live cortical bone in murine models of osteomyelitis. *J Bone Miner Res* 32:985–990. <https://doi.org/10.1002/jbmr.3055>
 55. Masters EA, Muthukrishnan G, Ho L, Gill AL, de Mesy Bentley KL, Galloway CA, McGrath JL, Awad HA, Gill SR, Schwarz EM. 2021. *Staphylococcus aureus* cell wall biosynthesis modulates bone invasion and osteomyelitis pathogenesis. *Front Microbiol* 12:723498. <https://doi.org/10.3389/fmicb.2021.723498>
 56. Masters EA, de Mesy Bentley KL, Gill AL, Hao SP, Galloway CA, Salminen AT, Guy DR, McGrath JL, Awad HA, Gill SR, Schwarz EM, Otto M. 2020. Identification of Penicillin Binding Protein 4 (PBP4) as a critical factor for *Staphylococcus aureus* bone invasion during osteomyelitis in mice. *PLoS Pathog* 16:e1008988. <https://doi.org/10.1371/journal.ppat.1008988>
 57. Liu X, Biboy J, Consoli E, Vollmer W, den Blaauwen T. 2020. MreC and MreD balance the interaction between the elongasome proteins PBP2 and RodA. *PLoS Genet* 16:e1009276. <https://doi.org/10.1371/journal.pgen.1009276>

58. Lamanna MM, Manzoor I, Joseph M, Ye ZA, Benedet M, Zanardi A, Ren Z, Wang X, Massidda O, Tsui H-C, Winkler ME. 2022. Roles of RodZ and class A PBP1b in the assembly and regulation of the peripheral peptidoglycan elongasome in ovoid-shaped cells of *Streptococcus pneumoniae* D39. *Mol Microbiol* 118:336–368. <https://doi.org/10.1111/mmi.14969>
59. Osipovitch DC, Therrien S, Griswold KE. 2015. Discovery of novel *S. aureus* autolysins and molecular engineering to enhance bacteriolytic activity. *Appl Microbiol Biotechnol* 99:6315–6326. <https://doi.org/10.1007/s00253-015-6443-2>